Analysis of NB Fast-Ion Loss Mechanisms in MHD Quiescent LHD Plasmas*)

Hideo NUGA[1)], Ryohsuke SEKI[1,2)], Kunihiro OGAWA[1,2)], Shuji KAMIO[1)], Yutaka FUJIWARA[1)], Hiroyuki YAMAGUCHI[1,2)], Masaki OSAKABE[1,2)], Mitsutaka ISOBE[1,2)], Sadayoshi MURAKAMI[3)] and Masayuki YOKOYAMA[1,2)]

[1)]*National Institute for Fusion Sciences, National Institutes of Natural Sciences, Toki 509-5292, Japan*
[2)]*The Graduate University for Advanced Studies, SOKENDAI, Toki 509-5292, Japan*
[3)]*Department of Nuclear Engineering, Kyoto University, Nishikyo, Kyoto 615-8540, Japan*

(Received 4 December 2020 / Accepted 10 February 2021)

Neutral beam (NB) fast-ion loss mechanisms in the large helical device (LHD) are investigated by the combination of the neutron measurement, the classical slowing-down simulation, and the neo-classical guiding center orbit following simulation. It is found that the neo-classical transport provides little contribution to the loss of tangentially injected NB fast-ions. For perpendicularly injected NB fast-ions, the neo-classical transport has more than 40% contribution to the NB fast ion loss. These results indicate that there are other loss mechanisms dominant in LHD plasmas. The charge exchange loss is one of the plausible candidates for the loss mechanism.

© *2021 The Japan Society of Plasma Science and Nuclear Fusion Research*

Keywords: fast ion confinement, neo-classical transport, charge exchange

DOI: 10.1585/pfr.16.2402052

1. Introduction

The burning fusion plasmas in fusion reactors are sustained by external heatings such as neutral beam injection (NBI) and radio-frequency waves and internal heating by fusion born α particles. The plasma heating is the kinetic power transfer from non-thermal energetic particles to the bulk thermal particles through Coulomb collision. Therefore, the high efficiency of the plasma heating requires sufficiently long confinement of the energetic particles until the kinetic energy of energetic particles is transferred. For this reason, numerous researchers have devoted themselves to this issue [1, 2].

Because the deuterium plasma experiment campaign started in the Large Helical Device (LHD) in March 2017 [3–6], neutron measurement has been available in LHD [7, 8]. The neutron measurement is one of the most important tools to investigate fast-ion confinement. This is because the fusion cross-section of the $D(d,n)^3He$ reaction has a strong dependence on the relative kinetic energy of reactant ions. Owing to the high injection energy of neutral beams (NBs) of up to 180 keV, the fusion reaction between energetic deuteron and thermal deuteron is dominant instead of the reaction between thermal deuterons in LHD [3]. This fact makes the fast-ion study using neutron measurement useful.

The fusion reaction rate of this kind of fusion reaction, the so-called "beam-thermal reaction," can be expressed as:

$$\mathcal{R}_{bt} = n_D \int \langle \sigma v \rangle_{bt} (T_D, E_{\mathrm{EP}}) f_{\mathrm{EP}}(\boldsymbol{v}_{\mathrm{EP}}) d\boldsymbol{v}_{\mathrm{EP}}, \quad (1)$$

where the subscript "D" and "EP" indicate the bulk deuteron and energetic deuteron. For these reasons, the neutron emission rate, S_n, reflects the velocity distribution of energetic deuteron.

In our previous study [9], the effective NB fast-ion confinement time has been investigated in LHD full-field magnetic configurations by using the neutron measurement and the classical slowing-down simulation. The effective confinement time can be estimated from the neutron decay time as shown in section 2. Although the effective confinement times for several configurations are estimated, the transport mechanism governing the fast-ion loss remains unclear. In this paper, the contribution of the neo-classical transport to the NB fast-ion loss is mainly investigated by the combination of the experimental result, the classical slowing-down simulation using CONV_FIT3D [9, 10], and the neo-classical guiding orbit following simulation using GNET [11, 12].

The rest of this paper consists of the following sections. In section 2, the experiment device and the experimental scenario are introduced. In section 3, the analysis method which extracts the contribution of the neoclassical-transport on the NB fast-ion loss is introduced. In section 4, the simulation codes used in this paper are explained. In section 5, simulation results are shown. Discussion of the disagreement with the analysis and the simulation results is in section 6. Section 7 concludes this pa-

author's e-mail: nuga.hideo@nifs.ac.jp

*) This article is based on the presentation at the 29th International Toki Conference on Plasma and Fusion Research (ITC29).

© 2021 The Japan Society of Plasma Science and Nuclear Fusion Research

per.

2. Experiment

To investigate the NB fast-ion confinement, we have performed short pulse NB injection experiments in LHD. The NBI system implemented in LHD [13] is shown in Fig. 1.

Figure 2 shows the typical waveform of this series of experiments. The short pulse (~40 ms) NBs are sequentially injected into plasmas. Each NB has different injection energy and direction to investigate the energy and direction dependence of the fast-ion confinement. The short pulse injection is chosen because the short pulse NBs have little impact on the bulk plasma parameters and have a lesser possibility to excite Magneto-Hydro-Dynamics (MHD) instabilities, which drive losses of fast-ions. In this series of experiments, the level of low-frequency magnetic fluctuations, which are detected by the magnetic probe set on the vacuum vessel, is $\delta B/B_t \sim 2\times10^{-5}$. This amplitude is sufficiently low for ignoring the fast-ion loss due to the magnetic fluctuations [14].

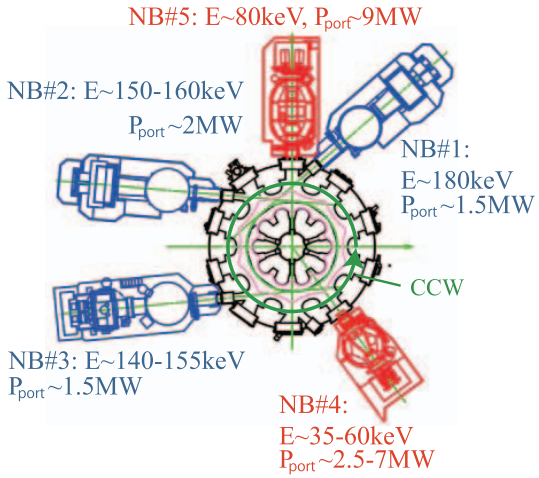

Fig. 1 The top view of the NBI system implemented in LHD is shown. NB#1-NB#3, which are the negative ion-based beams, are tangentially injected and, NB#4 and NB#5, which are positive ion-based beams, are perpendicularly injected. In this paper, the direction of the magnetic field line is counter-clockwise (CCW). Therefore, NB#1 and NB#3 are co-direction to the magnetic field line. Typical beam injection energies and powers are also displayed.

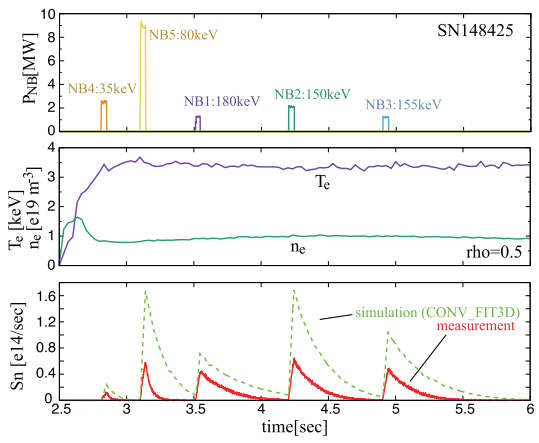

Fig. 2 The typical waveform of this series of experiments is shown. The injection powers and energies of NBs, the electron temperature and density on $\rho = 0.5$, and the neutron emission rate, S_n, are indicated. Solid and dashed curves in the bottom figure indicate the measured and simulated neutron emission rates. Simulation ignores the fast-ion loss.

The neutron emission rate S_n, shown in the bottom of Fig. 2, increases linearly after NBs are turned on and decreases exponentially after NBs are turned off. Here, we focus on the neutron decay time, τ_n. It is considered that two factors contribute to the decay of the neutron emission rate. One is the reduction of the fusion cross-section due to the fast-ion slowing-down. Within the range of beam energy, the fusion cross-section increases monotonically with the beam energy. For this reason, the neutron emission rate decays monotonically as the fast ion slowing-down. The other is the reduction of the fast ion density due to the fast-ion losses. Therefore, the decay of the neutron emission rate can be expressed as below.

$$\frac{dS_n}{dt} = -\frac{S_n}{\tau_n^{\mathrm{EXP}}} = -\frac{S_n}{\tau_n^{\mathrm{SD}}} - \frac{S_n}{\tau_c}, \tag{2}$$

where τ_n^{SD} and τ_c indicate the neutron decay time due to the slowing-down and the neutron decay time due to the fast-ion loss. Therefore, the relation between τ_n^{EXP}, τ_n^{SD}, and τ_c is given by:

$$\left(\tau_n^{\mathrm{EXP}}\right)^{-1} = \left(\tau_n^{\mathrm{SD}}\right)^{-1} + (\tau_c)^{-1}. \tag{3}$$

The slowing-down process of NB fast-ions owing to the classical Coulomb collisions can be estimated easily by the Fokker-Planck simulation, which ignores the NB fast-ion losses. Therefore, we can estimate the neutron decay time due to the classical slowing-down process, τ_n^{SD}. The simulation result of the neutron emission rate ignoring the NB fast-ion loss is shown at the bottom of Fig. 2. By using the relation expressed in eq. (3), we can estimate the neutron decay time due to the NB fast-ion losses, τ_c.

If we assume the effective confinement time, τ_c^{eff}, is constant in each magnetic configuration, the effective confinement time can be estimated by the weighted least mean square fitting in $\tau_n^{\mathrm{EXP}} = \tau_c^{\mathrm{eff}}\tau_n^{\mathrm{SD}}/(\tau_c^{\mathrm{eff}} + \tau_n^{\mathrm{SD}})$ (See Fig. 3). In our previous study [9], τ_c^{eff} for the typical magnetic configurations in LHD around $B_t \sim 2.75$ T have been obtained. However, the loss mechanism, which dominates τ_c^{eff} remains unclear. To clarify the loss mechanism, the following analyses are performed.

3. Analysis Method

In MHD quiescent tokamak plasmas, it is known that the neutron decay time can be explained by the neo-classical orbit following simulation [15]. The poor confinement of the perpendicular NB fast-ion can be often explained by the neo-classical transport induced by the strong ripple of the magnetic field line. Therefore, at first, we attempt to estimate the neutron decay time due to the neo-classical transport, τ_n^{NC}.

The simulation result of the neutron decay time by the orbit following code, τ_n^{OF}, usually includes the contribution both of the slowing-down and the neo-classical transport. Because it is difficult to separate these two contributions in the orbit following code, we divide them by comparing two simulation results, the slowing-down simulation, τ_n^{SD}, and the orbit following simulation, τ_n^{OF}. The difference between these two simulation results indicates the contribution of neo-classical transport. Therefore, τ_n^{NC} can be expressed as

$$\left(\tau_n^{\mathrm{OF}}\right)^{-1} - \left(\tau_n^{\mathrm{SD}}\right)^{-1} = \left(\tau_n^{\mathrm{NC}}\right)^{-1}. \tag{4}$$

Here, it is noted that the radial transport due to the slowing-down in the non-uniform magnetic field is classified as neo-classical transport. This is because the slowing-down simulation calculates only the energy dissipation and does not include the orbit shift due to the slowing-down. In this paper, two simulation codes CONV_FIT3D and GNET are used to estimate τ_n^{SD} and τ_n^{OF}.

4. Simulation Codes

To estimate τ_n^{SD}, VMEC [16], FIT3D (composed of HFREYA, MCNBI, and FIT) [17–20], and CONV_FIT3D have been used. These codes are one of the components of the integrated transport analysis suite TASK3D-a [21]. VMEC calculates the three-dimensional magnetic equilibrium. According to the obtained configuration, NB fast-ion birth profile is calculated by FIT3D. At the step of beam ion birth calculation, FIT3D follows NB fast-ion orbits for a few tens of microseconds to consider the NB fast-ion prompt loss and the NB birth profile broadening due to the finite orbit width effect. For positive ion-based beams, the full, half, and one-third energy fractions of injected neutral particles are assumed to be typical values, 0.78, 0.16, and 0.06, respectively.

CONV_FIT3D code calculates the NB fast-ion slowing-down process to obtain the energy distribution of NB fast-ions. In this code, the orbit deviation from the magnetic surface is neglected. Additionally, transport across the magnetic surface during the slowing-down process is also ignored. Because the following discussion requires the comparison of the simulation results between CONV_FIT3D and GNET, the collision model implemented in CONV_FIT3D has been refined from the model used in ref. [9] to be the same as the model implemented in GNET. The refined slowing-down equation based on the non-relativistic background Maxwellian approximation without $v_{\mathrm{EP}} \ll v_{\mathrm{th},e}$ assumption is given by

$$\frac{dE}{dt} = -\frac{2}{\tau_{se}} Z_{\mathrm{EP}}^2 E^{-1/2} \left[\frac{3\pi^{1/2} m_{\mathrm{EP}}^{3/2} T_e^{3/2}}{4 m_e^{1/2}} \times \left(\frac{g(u_e)}{m_e} + \sum_i \frac{Z_i^2 n_i}{n_e m_i} g(u_i) \right) \right], \tag{5}$$

$$\tau_{se} = \frac{3(2\pi)^{3/2} \epsilon_0^2 m_{\mathrm{EP}} T_e^{3/2}}{n_e e^4 m_e^{1/2} \ln \Lambda}, \tag{6}$$

$$g(u_s) = \mathrm{erf}(u_s) - u_s \mathrm{erf}'(u_s), \tag{7}$$

$$\mathrm{erf}(u_s) = \frac{2}{\pi} \int_0^{u_s} \exp(-x^2) dx, \tag{8}$$

$$\mathrm{erf}'(u_s) = \frac{2}{\pi} \exp(-u_s^2), \tag{9}$$

$$u_s = \frac{v_{\mathrm{EP}}}{v_{s,\mathrm{th}}}, \tag{10}$$

where τ_{se} is the Spitzer slowing-down time on electron, the subscripts "s", "e", "i", and "EP" indicate the particle species, $v_{\mathrm{th},s} = \sqrt{T_s/m_s}$ is the thermal velocity of "s", and $u_s = v_{\mathrm{EP}}/v_{\mathrm{th},s}$, respectively. Here, we assume $T_i = T_e$. This slowing-down equation corresponds to the slowing-down term implemented in GNET.

GNET code, which solves the drift kinetic equation by using the Monte Carlo method, is used to estimate τ_n^{OF} instead of CONV_FIT3D code. In GNET, the behavior of the test particle guiding center orbit is described in the Boozer coordinate, which is constructed from VMEC equilibrium. GNET takes the NB birth profile calculated by FIT3D as input. The velocity diffusion term and slowing-down term of test particles are calculated by the Monte Carlo method equivalent to the Lorentz collision operator. The implemented collision operator assumes non-relativistic background Maxwellian. The equilibrium and background plasma parameters are assumed to be constant during the calculation. For this reason, the plasma parameters when each NB is turned off are used for the calculation.

Among these codes, the electron density and temperature profiles measured by Thomson scattering diagnostic system [22, 23] are taken as input. The ion ratio between proton and deuteron, $n_{\mathrm{D}}/(n_{\mathrm{H}} + n_{\mathrm{D}})$, and the ratio between hydrogen and helium ions, $n_{\mathrm{He}}/(n_{\mathrm{H}} + n_{\mathrm{D}} + n_{\mathrm{He}})$, are also taken into account. Because the other ion species such as carbon are not taken into account in the following calculation, the effective charge assumed in this calculation is underestimated. The typical value of the effective charge assumed in this calculation is approximately $Z_{\mathrm{eff}} \sim 1.2$. The measurement of the effective charge can not be used owing to the insufficient plasma density.

In this paper, CONV_FIT3D and GNET implement the same model of the fusion cross-section. Because the fusion reaction between NB fast-deuteron and bulk deuteron is dominant, the fusion reaction rate can be reduced into beam-thermal reaction as eq. (1). For the fusion reactivity, $\langle \sigma v \rangle_{bt}$, the approximated expression derived by Mikkelsen [24] is used. The fitting coefficients required for

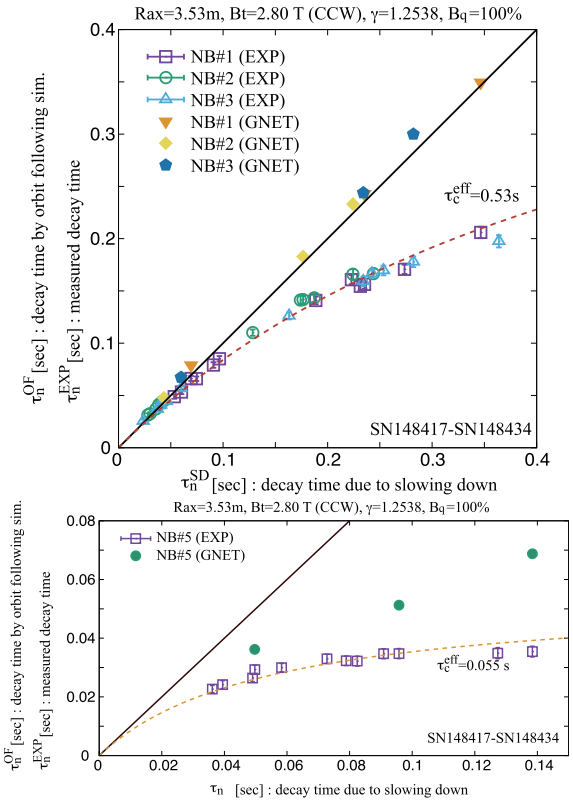

Fig. 3 Experimentally observed neutron decay time and simulated neutron decay time by GNET are plotted against the simulated neutron decay time by CONV_FIT3D in (R_{ax}, B_t) = (3.53 m, 2.80 T) configuration. The pitch parameter of the helical coil is $\gamma = 1.2538$ and the quadrupole magnetic field is $B_q = 100\%$. These two values are also used for other configurations. The top figure shows the relation for tangential NB fast-ions and the bottom figure shows the relation for perpendicular NB fast-ions. Dashed fitting curves are $\tau_n^{EXP} = 0.53\tau_n^{SD}/(0.53+\tau_n^{SD})$ for tangential case and $\tau_n^{EXP} = 0.055\tau_n^{SD}/(0.055+\tau_n^{SD})$ for perpendicular case, respectively.

the fusion reactivity are chosen from the reference [25].

5. Simulation Results

Figure 3 shows the relation between the experimentally measured neutron decay time τ_n^{EXP} and simulated neutron decay time due to the fast-ion slowing-down, τ_n^{SD} in (R_{ax}, B_t) = (3.53 m, 2.80 T) configuration. Besides, the simulated neutron decay time by GNET, τ_n^{OF} is also displayed. In this figure, the value of the electron density is with the range of $\sim 0.8 \times 10^{19}\,\mathrm{m}^{-3} < n_e(\rho = 0.5) < \sim 3 \times 10^{19}\,\mathrm{m}^{-3}$. Unlike the experimental results, simulation results of tangential beams by GNET almost satisfy the relation $\tau_n^{OF} = \tau_n^{SD}$. This result indicates that the neo-classical transport has little contribution to the NB fast-ion loss for tangential beams. On the contrary, GNET results for perpendicular beam are separated from $\tau_n^{OF} = \tau_n^{SD}$ line. Because GNET results do not obey also the fitting curve, it is considered that the neo-classical transport has an unignorable impact on the NB fast-ion loss.

Table 1 For the perpendicular beams, the neutron decay times due to the slowing-down, the neo-classical transport, and the ratio of the neo-classical transport to the effective confinement time are listed for three configurations.

# discharge	R_{ax} [m]	τ_n^{SD} [s]	τ_n^{NC} [s]	τ_n^{rest} [s]	R_c^{NC}
148425	3.53	0.140	0.135	0.0983	0.41
148432	3.53	0.0507	0.126	0.104	0.45
139595	3.6	0.0755	0.151	0.0967	0.39
139600	3.6	0.0344	0.0842	0.197	0.70
139612	3.75	0.0787	0.0768	0.135	0.64
139621	3.75	0.0220	0.0401	-0.219	1.22

Since the inverse of the fast-ion confinement time $(\tau_c)^{-1}$ consists of the contribution of neo-classical transport $(\tau_n^{NC})^{-1}$ and the rest of the fast-ion loss mechanism $(\tau_n^{rest})^{-1}$, the ratio of the neo-classical transport to the fast-ion loss can be described by $R_c^{NC} = (\tau_n^{NC})^{-1}/(\tau_c)^{-1}$. If the value of $\tau_c^{eff} = 0.055$ s is chosen as the value of τ_c, the ratio of the neo-classical transport to the fast-ion loss for NB#5 in each discharge can be estimated. In this configuration, the values of the ratio are approximately $R_c^{NC} \sim 0.4$ - 0.5.

It is noted that the result of NB#4 is omitted in Fig. 3. This is because the simulation result of CONV_FIT3D for NB#4 is not reliable. In discharges of this configuration, NB#4 has untypically low injection energy $E_b \sim 35$ keV. When the energy of the NB fast-ion is close to the bulk temperature, the velocity diffusion effect, which is neglected in CONV_FIT3D, can not be ignorable. Because the velocity diffusion effect is taken into account by GNET and is significant at the low energy range such as the NB#4 case, the difference of the simulated neutron decay time between GNET and CONV_FIT3D does not indicate the contribution of the neo-classical transport. For this reason, the result for NB#4 is omitted.

Similar analyses have been performed for the other configurations, (R_{ax}, B_t) = (3.6 m, 2.75 T) and (3.75 m, 2.64 T). Even in outward shifted plasmas, the neutron decay time of tangential NB fast-ions estimated by GNET, τ_n^{OF} approximately equals the neutron decay time of tangential NB fast-ions estimated by CONV_FIT3D, τ_n^{SD}. Therefore, the contribution of the neo-classical transport to the tangentially injected NB fast-ions can be negligible. Table 1 shows the results of the analysis estimating τ_n^{NC} for perpendicular beams in the three configurations, (R_{ax}, B_t) = (3.53 m, 2.80 T), (3.6 m, 2.75 T) and (3.75 m, 2.64 T). The values of τ_c^{eff}, which are used for estimating R_c^{NC}, in each configuration are 0.055 s, 0.059 s, and 0.049 s, respectively. Table 1 has two data, which have different τ_n^{SD}, in each magnetic configuration.

From Table 1, it is found that τ_n^{NC} becomes shorter in $R_{ax} = 3.75$ m configuration. In LHD plasmas, it has been investigated numerically [26] that the neo-classical diffusion coefficient increases as the plasma shifts outward. The result in Table 1 is consistent qualitatively with the previ-

ous numerical result. The values of R_c^{NC} are within the range of $0.4 < R_c^{\mathrm{NC}} < 0.7$ except for the bottom discharge. From this result, even for perpendicular beam ions, the neo-classical transport can not explain all of the fast-ion loss.

It is noted that the value of R_c^{NC} in the case of $(R_{\mathrm{ax}}, \tau_n^{\mathrm{SD}}) = (3.75\,\mathrm{m}, 0.0220\,\mathrm{s})$ exceeds unity. It can be considered that GNET over-estimates the fast-ion losses in the outward shifted configuration. This is because GNET stops the orbit following calculation when the test particle crosses the last closed flux surface (LCFS). In actual plasmas, however, LCFS is not always the confinement/loss boundary for energetic ions. Energetic ions can re-enter the area inside the LCFS after passing through the area outside the LCFS. This is because the orbit of energetic ions deviates from the magnetic surface due to the effect of the so-called finite orbit width effect. The lack of the re-entering effect can lead to the over-estimation of fast-ion losses [27, 28].

6. Discussion

The investigation of the rest component of the fast-ion loss mechanisms is required. The second candidate of the loss mechanism is the charge exchange (CX) loss. In the previous paper [9], experimental data in the long τ_n^{SD} region were omitted. This is because that the different trend, which can be explained by the CX loss, appeared in the long τ_n^{SD} region. To investigate the contribution of CX loss in the short τ_n^{SD} region, additional simulations are performed in this section.

Although the CX reactivity depends on the neutral gas density linearly, the measurement of the neutral gas density profile is difficult. Besides, since the neutral gas density profile changes exponentially in ρ space, the value of the neutral gas density profile has a wide range. For these reasons, the quantitative discussion of the CX loss is also difficult. Therefore, in this paper, we attempt a simple evaluation of the CX loss contribution as follows.

In the core region of LHD plasmas, the neutral gas density profile has a negative dependence on the electron density [29,30]. For this reason, if the plasma electron density is constant during the discharge, it is considered that the neutral gas density profile is also constant during the discharge. Here, we focus on the discharge shown in Fig. 2 because this discharge has a constant electron density in time. In the following GNET calculation, the neutral gas density profile assumes to be $n_0(\rho) = C \times n_0^{\mathrm{sample}}(\rho)$, where C is the arbitrary constant and $n_0^{\mathrm{sample}}(\rho)$ is the sample profile of the neutral gas density shown in Fig. 4.

If the rest component of the loss mechanism can be explained by the CX loss and the assumed neutral gas density is correct, the ratio $\tau_n^{\mathrm{OF}}/\tau_n^{\mathrm{EXP}}$ becomes unity in each beam with the same value of C. It is noted that τ_n^{OF} in this section includes the CX loss effect. Figure 5 shows the dependence of $\tau_n^{\mathrm{OF}}/\tau_n^{\mathrm{EXP}}$ on the arbitrary density factor

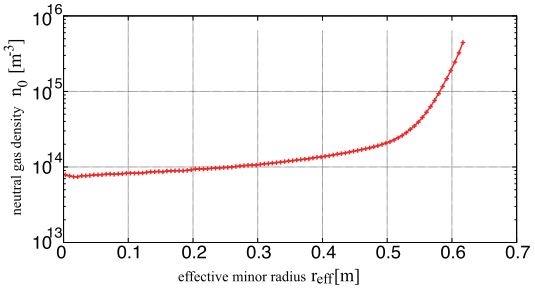

Fig. 4 The neutral gas density profile assumed in the simulation is shown. This profile is calculated by AURORA code [31] for the case in which the core electron density is approximately 1.5×10^{19} m^{-3}. The plasma minor radius is approximately $a = 0.61$ m.

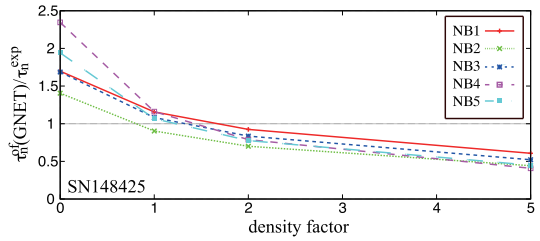

Fig. 5 The ratio τ_n^{EXP} to τ_n^{OF} is plotted against the density factor C.

C. From Fig. 5, the ratio in each beamline except NB#2 becomes unity with $C \sim 1.5$. NB#2, which has a counter direction to the magnetic field line, has a smaller density factor that satisfies $\tau_n^{\mathrm{OF}}/\tau_n^{\mathrm{EXP}} = 1$ as compared to the other beamlines. If we chose the value of $C = 1.5$, the value of $\tau_n^{\mathrm{OF}}/\tau_n^{\mathrm{EXP}}$ for NB#2 is less than unity. This result indicates that the NB#2 fast-ions have felt higher neutral gas density in the GNET simulation rather than in the actual plasma. Because fast-ions, which have a counter direction to the magnetic field, shift outward in ρ space, the actual neutral gas density profile is considered to be flatter than the profile assumed in this simulation. The assumed neutral gas density profile, which is shown in Fig. 4, is obtained for higher core electron density plasmas rather than the actual plasma. The lower electron density plasma tends to have a flatter neutral gas density profile due to the long penetration depth of neutral particles. Therefore, the smaller value of C for NB#2 is qualitatively consistent.

Although the discussion in this section is too simplified, it can clarify that the CX loss plays an important role in the fast-ion loss even in the short τ_n^{SD} region. Detailed discussion is to be found in future work.

7. Conclusion

We have investigated the NB fast-ion loss mechanism in MHD quiescent LHD plasmas by using neutron measurement and simulations. The contribution of the neo-classical transport to the NB fast-ion loss is mainly dis-

cussed because it has been denoted that the orbit following simulation can explain the NB fast-ion confinement in the previous work in tokamak [15]. In this paper, the contribution of the neo-classical transport to the NB fast-ion loss is investigated by the combination of the experimental result, the classical slowing-down simulation using CONV_FIT3D [9, 10], and the neo-classical guiding orbit following simulation using GNET [11, 12].

In our previous research [9], the decay of the neutron emission rate is separated into two factors. One is the reduction of the fusion cross-section due to the NB fast-ion slowing-down. The other is the reduction of the NB fast-ion density due to the NB fast-ion loss. In some LHD full-field configurations, the contributions of the NB fast-ion loss to the neutron decay, $\tau_c^{\rm eff}$, have been estimated. In this paper, we investigated the loss mechanism which governs the $\tau_c^{\rm eff}$.

From analysis results in section 5, it is found that the neo-classical transport provides little contribution to the decay of the neutron emission rate for tangential NB fast-ions in LHD full-field three configurations, $(R_{\rm ax},\ B_t) = (3.53\,{\rm m},\ 2.80\,{\rm T})$, $(3.6\,{\rm m},\ 2.75\,{\rm T})$, and $(3.75\,{\rm m},\ 2.64\,{\rm T})$. For perpendicularly injected NB fast-ions, the neo-classical transport has more than 40% contribution to the NB fast-ion loss. This percentage becomes larger in outward shifted plasmas. It is noted that since GNET can not take the re-entering effect into account, the percentage might be over-estimated in outward shifted plasmas. These results indicate that half of the contribution to the fast-ion loss for perpendicular NBs and almost the full contribution to the fast-ion loss for tangential NBs are governed by the other transport mechanisms. The next candidate for the transport mechanisms is the charge exchange loss. The contribution of the charge exchange loss to the NB fast-ion loss is simply discussed in section 6. In this discussion, we found the consistent neutral gas density in each beam, if we assume the rest of the contribution of the NB fast-ion loss is the charge exchange loss. Therefore, it can be considered that the charge exchange loss plays an important role in the NB fat-ion loss. The detailed analyses considering the charge exchange loss are future work.

Acknowledgments

This work is supported partly by LHD project budgets (NIFS07KLPH004, NIFS18KNSR007, and NIFS14KNTT025).

[1] W. Heidbrink and G. Sadler, Nucl. Fusion **34**, 535 (1994).
[2] N.N. Gorelenkov, S. Pinches and K. Toi, Nucl. Fusion **54**, 125001 (2014).
[3] M. Osakabe, Y. Takeiri, T. Morisaki *et al.*, Fusion Sci. Technol. **72**, 199 (2017).
[4] Y. Takeiri, IEEE Trans. Plasma Sci. **46**, 1141 (2018).
[5] M. Osakabe, M. Isobe, M. Tanaka *et al.*, IEEE Trans. Plasma Sci. **46**, 2324 (2018).
[6] Y. Takeiri, IEEE Trans. Plasma Sci. **46**, 2348 (2018).
[7] M. Isobe, K. Ogawa, T. Nishitani *et al.*, IEEE Trans. Plasma Sci. **46**, 2050 (2018).
[8] K. Ogawa, M. Isobe, T. Nishitani *et al.*, Nucl. Fusion **59**, 076017 (2019).
[9] H. Nuga, R. Seki, K. Ogawa *et al.*, J. Plasma Phys. **86**, 815860306 (2020).
[10] H. Nuga, R. Seki, K. Ogawa *et al.*, Plasma Fusion Res. **14**, 3402075 (2019).
[11] S. Murakami, H. Yamada, M. Sasao *et al.*, Fusion Sci. Technol. **46**, 241 (2004).
[12] H. Yamaguchi and S. Murakami, Nucl. Fusion **56**, 026003 (2015).
[13] Y. Takeiri, O. Kaneko, K. Tsumori *et al.*, Fusion Sci. Technol. **58**, 482 (2010).
[14] K. Ogawa, M. Isobe, K. Toi *et al.*, Nucl. Fusion **50**, 084005 (2010).
[15] K. Tobita, K. Tani, T. Nishitani *et al.*, Nucl. Fusion **34**, 1097 (1994).
[16] S.P. Hirshman and J. Whitson, Phys. Fluids **26**, 3553 (1983).
[17] S. Murakami, N. Nakajima and M. Okamoto, Trans. Fusion Technol. **27**, 256 (1995).
[18] M. Sato, S. Murakami, A. Fukuyama *et al.*, Proc. 18th Int. Toki Conf. 2008.
[19] P. Vincenzi, T. Bolzonella, S. Murakami *et al.*, Plasma Phys. Control. Fusion **58**, 125008 (2016).
[20] R. Seki, K. Ogawa, M. Isobe *et al.*, Plasma Fusion Res. **14**, 3402126 (2019).
[21] M. Yokoyama, R. Seki, C. Suzuki *et al.*, Nucl. Fusion **57**, 126016 (2017).
[22] K. Narihara, I. Yamada, H. Hayashi *et al.*, Rev. Sci. Instrum. **72**, 1122 (2001).
[23] I. Yamada, K. Narihara, H. Funaba *et al.*, Fusion Sci. Technol. **58**, 345 (2010).
[24] D. Mikkelsen, Nucl. Fusion **29**, 1113 (1989).
[25] H.-S. Bosch and G. Hale, Nucl. Fusion **32**, 611 (1992).
[26] S. Murakami, A. Wakasa, H. Maaßberg *et al.*, Nucl. Fusion **42**, L19 (2002).
[27] K. Hanatani and F.-P. Penningsfeld, Nucl. Fusion **32**, 1769 (1992).
[28] R. Seki, K. Watanabe, H. Funaba *et al.*, Nucl. Fusion **53**, 063016 (2013).
[29] K. Fujii, M. Goto, S. Morita *et al.*, Nucl. Fusion **55**, 063029 (2015).
[30] M. Goto, K. Sawada, T. Oishi *et al.*, Plasma Phys. Control. Fusion **58**, 084001 (2016).
[31] M. Hughes and D. Post, J. Comput. Phys. **28**, 43 (1978).